Performance of a Deep Excavation Irregular Supporting Structure Subjected to Asymmetric Loading

Liu, Shouhua; Yang, Junsheng; Fu, Jinyang; Zheng, Xiangcou

DOI
10.1061/(ASCE)GM.1943-5622.0001468

Publication date
2019

Document Version
Final published version

Published in
International Journal of Geomechanics

Citation (APA)
Liu, S., Yang, J., Fu, J., & Zheng, X. (2019). Performance of a Deep Excavation Irregular Supporting Structure Subjected to Asymmetric Loading. *International Journal of Geomechanics*, *19*(7), Article 05019007. https://doi.org/10.1061/(ASCE)GM.1943-5622.0001468

Case Study

Performance of a Deep Excavation Irregular Supporting Structure Subjected to Asymmetric Loading

Shouhua Liu[1]; Junsheng Yang[2]; Jinyang Fu[3]; and Xiangcou Zheng[4]

Abstract: Because of the extreme terrain limitations and heavy traffic in congested urban areas, the supporting structures for deep excavations often undergo an asymmetric loading condition at two sides. This article reports the results of an investigation based on detailed numerical modeling of the supporting scheme and mechanical performance of a deep excavation of a metro station having different elevations at two sides. The two proposed types of design schemes for support and excavation were discussed and analyzed to evaluate the suitability of using regular or irregular supporting structures. The mechanical performance of the adopted supporting scheme was then evaluated using three-dimensional numerical analysis and verified via field observations. The results show that the irregular supporting structure functions satisfactorily when subjected to asymmetric loading, and it can also realize semicovered excavation in narrow and congested downtown areas to effectively solve the problem of traffic. The solution presented in this study can provide valuable references for the design of urban deep excavations with an asymmetric side elevation. **DOI: 10.1061/(ASCE)GM.1943-5622.0001468.** © *2019 American Society of Civil Engineers.*

Author keywords: Deep excavation; Irregular supporting structure; Regular supporting structure; Asymmetric loading; Numerical analysis.

Introduction

Deep excavations are frequently performed in practical engineering to meet the increasing needs of public transportation, rail transit, business, and parking. The limited urban space and heavy traffic render the surrounding environment of deep excavations extremely complicated (Zhang et al. 2018). Excessive movement of the retaining structures and the ground can lead to damage of the adjacent structures and loss of lives. To ensure the safety of deep excavations and the surrounding environment, the deformation and stress distribution characteristics for the supporting structures of the deep excavation are of particular interest for engineers.

After Peck (1969), many scholars have made significant contributions to clarifying the performance of deep excavations supported by a diaphragm wall with multistruts. Ou et al. (1998) carried out a field test for a deep excavation process using the top-down construction method in Taipei. They found that the magnitudes of the deflection increased with an increase in the excavation depth. Field tests and numerical methods were employed by Kim and Lee (2005) to investigate the performance of a cylindrical diaphragm wall and ground movement; they also determined the relationship between the wall stiffness and performance of a cylindrical diaphragm wall. Liu et al. (2005) analyzed the mean values of the maximum lateral displacements using different construction methods through 300 deep excavations of soft soil in Shanghai. They concluded that the wall displacement was negatively correlated with the factor of safety against basal heave and supporting-system stiffness. Studies have also been conducted to investigate the performance of the excavation of soft soil areas in Shanghai, China, through measured data (e.g., Tan and Li 2011; Yang and Liu 2017).

Because of the extreme terrain and heavy traffic in congested urban areas, deep excavation is usually performed in a complex and dangerous state of stress. Numerical modeling is an important means to compare and select the appropriate supporting scheme for deep excavation. Meanwhile, numerical modeling is also employed to predict the performance of the deep excavation process. To predict the performance of the excavation more accurately, finite-element analyses have been carried out previously to simulate the construction of such complex excavations (e.g., Hou et al. 2009; Nogueira et al. 2011; Shao and Macari 2008). Yoo and Lee (2008) used numerical modeling to study the characterization of ground-surface movements induced by deep excavation. The finite-element method has also been used for the analysis and design of partial ground improvement in deep excavations (e.g., Ou et al. 2008; Chowdhury et al. 2013; Arai et al. 2008).

The aforementioned studies pertaining to the current state of the art clearly demonstrate that the performance of the supported deep excavation system in case of the same elevation at two sides has been extensively investigated and that the principle for design is perspicuous. However, because of the extreme terrain limitations and heavy traffic in congested urban areas, excavation must be performed with different elevations at the two sides, which results in an asymmetric loading condition and leads to the supporting structure exhibiting irregular behavior. However, few studies have focused on this issue (Shi et al. 2011), and even then, they only discussed the situation of a regular supporting system resisting the

[1]Ph.D. Candidate, School of Civil Engineering, Central South Univ., Changsha 410075, People's Republic of China. ORCID: https://orcid.org/0000-0002-6045-9353

[2]Professor, School of Civil Engineering, Central South Univ., Changsha 410075, People's Republic of China (corresponding author). Email: jsyang@csu.edu.cn

[3]Associate Professor, School of Civil Engineering, Central South Univ., Changsha 410075, People's Republic of China. ORCID: https://orcid.org/0000-0002-0632-1222

[4]Ph.D. Candidate, Civil Engineering and Geoscience, Delft Univ. of Tech., Mekelweg 5, Delft 2628 CD, Netherlands.

Note. This manuscript was submitted on July 19, 2018; approved on March 5, 2019; published online on May 7, 2019. Discussion period open until October 7, 2019; separate discussions must be submitted for individual papers. This paper is part of the ***International Journal of Geomechanics***, © ASCE, ISSN 1532-3641.

asymmetric loading. Moreover, it is of great engineering significance to design an irregular supporting system for deep excavation cases involving asymmetric loading, and field measurements are required to be performed to enable the maturing of the design theory and experience.

This study presents an investigation of the supporting scheme and mechanical performance of the deep excavation of a metro station having different elevations at the two sides and complex surrounding traffic conditions by using detailed numerical modeling. The proposed two types of design schemes for the support and excavation were discussed and analyzed to evaluate the suitability of using a regular or irregular supporting structure. A case study considering the project of Changsha Subway Line 4 was carried out to evaluate the performance of the adopted irregular supporting structure by using numerical analysis and field measurements. A good agreement was found between the numerical results and field data, which not only indicates the effectiveness of the adopted irregular supporting structure but also highlights its advantages.

Project Overview

The location for the investigated deep excavation for the Shazitang Station of Subway Line 4 is the Tianxin Area of Changsha. Fig. 1 presents the site plan for the project. The investigated deep excavation lies along the Huangtuling Road, with Shaoshan Road to the west. The deep excavation area has a length of 169.6 m, with its width and depth, respectively, varying from 22.9 to 44.1 m and from 26.8 to 29.5 m. The excavation zone is composed mainly of silty clay, sandy gravel, and argillaceous siltstone (Fig. 2).

On the south side of the excavation, 17-story RC frame structures and a 5-story brick–concrete structure are installed next to Huangtuling Road. These three buildings are all supported by the pile foundation. The distance between the deep excavation and the buildings varies between 7 and 25 m (Fig. 1). The ground elevations of the excavation on the south and north sides are 78 and 74 m, respectively. Thus, the deep excavation is subjected to asymmetric loading.

Options for Supporting Scheme

For deep excavations subjected to asymmetric loading, two different optional supporting schemes, namely, a regular supporting structure and an irregular supporting structure (Fig. 2), are considered. The difference between these two supporting schemes is the type of the first strut. The first strut of the regular supporting structure is straight bracing, whereas the irregular supporting structure is composed of straight bracing and inclined bracing.

The designed supporting schemes consist of a diaphragm wall with four struts, placed 0, 7, 14.5, and 18.5 m below the lower ground surface (BLGS). The RC structure is employed for the first and third struts, with their cross sections being 1×1.2 m and 1.2×1.3 m, respectively. The first and third struts are horizontally spaced 6 m along the longitudinal direction of the excavation. The second and fourth struts are steel pipes with a horizontal spacing distance of 3 m. The cross section of the steel pipe has an external diameter of 609 mm and a thickness of 16 mm. All steel pipes were preloaded with a 500-kN load. The thickness of the diaphragm wall is 1 m. When the diaphragm wall is located in low ground elevations, it is termed the *north wall*; otherwise, it is named as the *south wall* (Fig. 2). The embedment depth of the wall into medium weathered rock is 3 m.

To increase the stiffness of the supporting system, erect column piles were installed in the excavation area at intervals of 3 m. The erect column piles were inserted 4 m into the uplift piles with a diameter of 1.2 m. The Young's moduli, E, of the concrete and steel used at this site are 3.2×10^7 kPa and 2.1×10^8 kPa, respectively.

Numerical Analysis of the Optimal Supporting Scheme

Three-Dimensional Finite-Element Model

Numerical analyses were carried out to determine the optimal supporting scheme. Fig. 3 presents two numerical models, which correspond to different supporting schemes. The model was composed of 71,010 nodes and 64,358 elements. To reduce the boundary effect, the model with dimensions of 180 m (X) $\times$ 90 m (Y) $\times$ 14 m (Z) (Fig. 3) was selected. A complete three-dimensional (3D) finite-

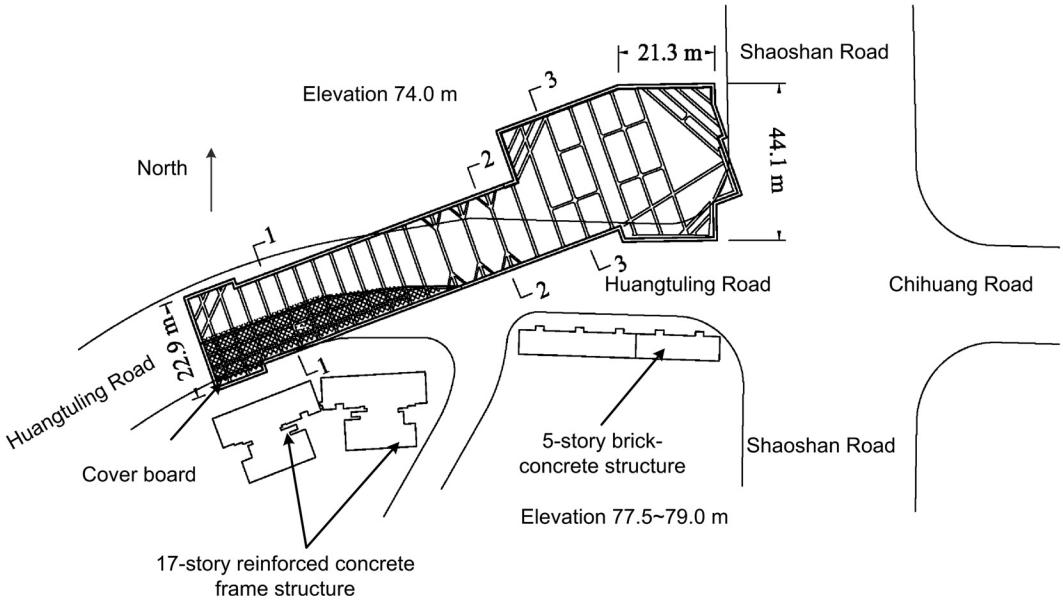

Fig. 1. Deep excavation layout.

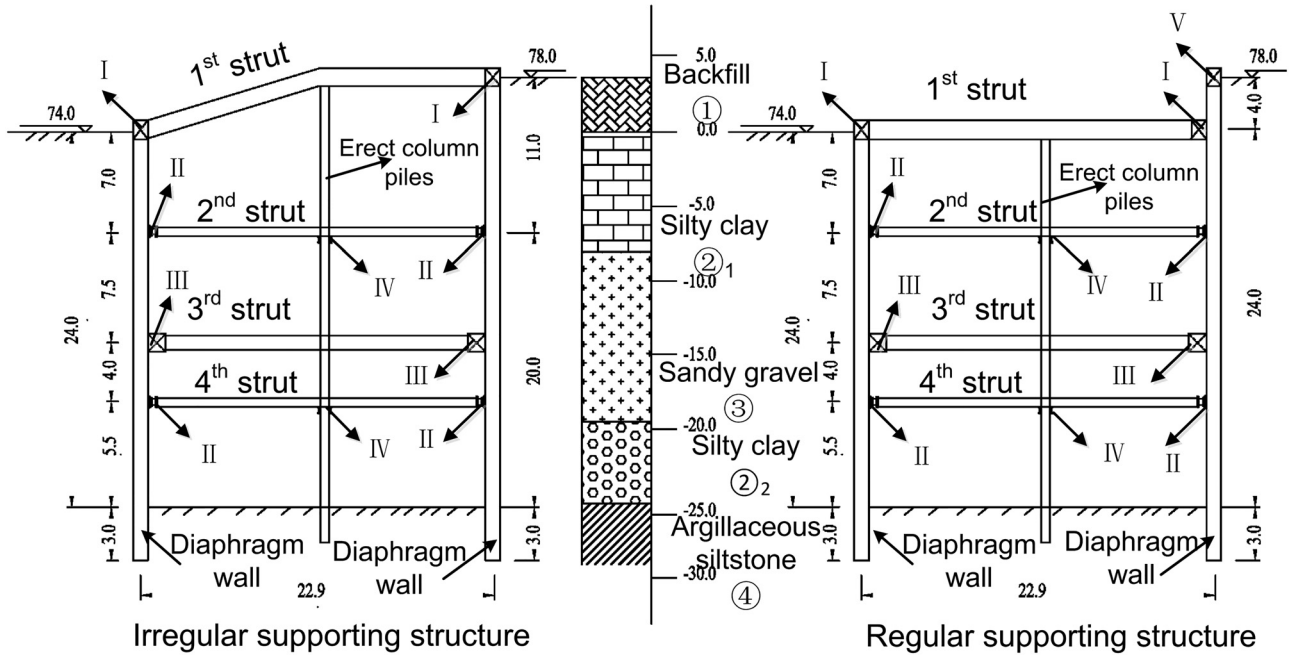

Fig. 2. Cross section of options for the supporting scheme (unit: m).

element (FE) model was generated considering diaphragm wall, struts, waist beams, erect column piles, and uplift piles.

Material Properties

Several advanced constitutive models are available, such as the UH model (Yao et al. 2008, 2009, 2012) and the disturbed-state-concept model (Desai 2015a, b) for clays and the bounding surface model for gravel (Xiao et al. 2014). However, this study aimed to evaluate the overall performance of the supporting structure for deep excavations subjected to asymmetric loading conditions rather than to investigate the constitutive soil behavior via laboratory test. Therefore, for simplicity, the Abaqus build-in and matured soil constitutive models, the modified Cam-clay (MCC) model, and the Mohr-Coulomb model were used for the numerical analysis in this study (Huang et al. 2011; Zhao et al. 2019a, b). The silty soil was modeled with a MCC plasticity model (as presented in Table 1) in this study. K refers to the ratio of the flow stress in triaxial extension to the flow stress in triaxial compression ($0.778 \le K \le 1$; $K = 1$ in the FE analysis of the current study). λ and κ are calculated using $C_c/2.303$ and $C_s/2.303$, respectively, where C_c and C_s denote the compression index and swelling index, respectively (Huang et al. 2011). M is taken from Zeng et al.'s (2017) article, in which the conventional parameters of soil are similar to those employed in the current study. The gravel and gravel soil layer were modeled with a Mohr-Coulomb elastoplastic model. Moreover, in the design stage, the RC support structure is governed by the sectional forces, deformation, and the overall stability, and no plastic yielding is allowed; therefore, the support structure is usually modeled as a linear elastic material, such as in the numerical simulation analysis of a deep excavation reported by Hashash et al. (2006), Arai et al. (2008), Hsieh et al. (2013), and Schwamb and Soga (2015). Hence, in this study, the diaphragm wall, struts, waist beams, erect column piles, and uplift piles were also simply simulated as linear isotropic elastic materials.

Boundary Conditions

The bottom boundary of the model was fixed vertically while the top surface was left free. The lateral sides of the model were fixed in the horizontal direction while vertical movement was allowed. In the numerical models, the struts and waist beams were modeled as beam elements, the erect column piles and uplift piles were considered as pile elements, and the diaphragm wall was considered as a shell element. The excavation sequence was simulated using the Model Null technique, which is consistent with the case in practical construction processes.

Comparison of the Two Supporting Schemes

Deflection of the Diaphragm Wall

Fig. 4 presents the final horizontal displacement curve of the diaphragm wall of the two supporting schemes. When the diaphragm wall deforms toward the interior of the deep excavation, the horizontal displacement of the diaphragm wall is positive. The maximum horizontal displacements (δ_{hmax}) of the irregular and regular supporting structures are 19.7 and 18.8 mm, respectively. The deformation mode and amplitude of the diaphragm wall of the two supporting schemes are approximately the same, except for those of the upper part of the south wall. The south wall of the regular supporting structure exhibits a cantilever deformation mode; however, for the irregular supporting structure, the south wall exhibits a compound

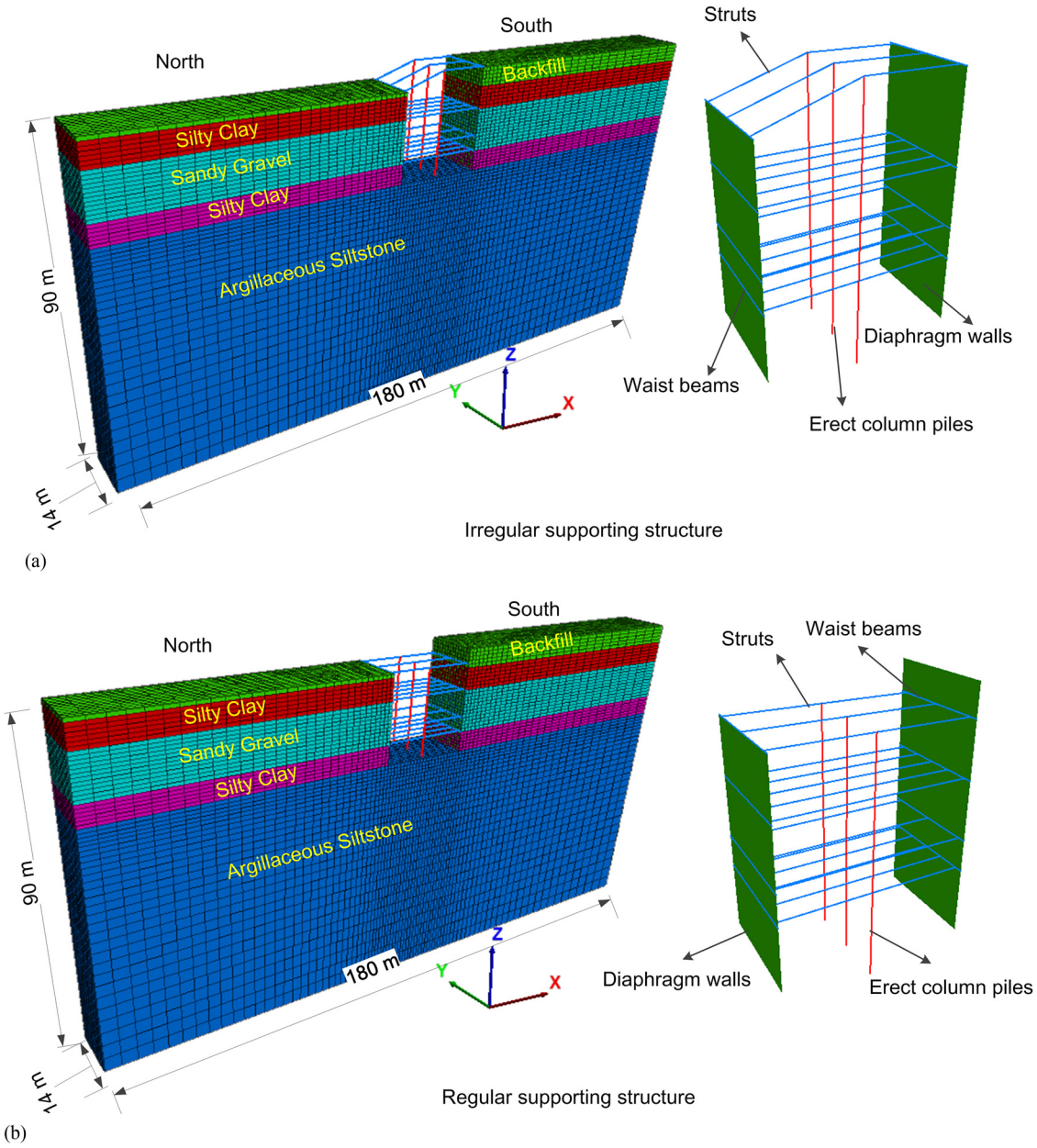

Fig. 3. 3D numerical models: (a) irregular supporting structure; and (b) regular supporting structure.

deformation mode (Fig. 4). The diaphragm wall can be regarded as a beam placed vertically. In the numerical model, the struts were rigidly connected to the diaphragm wall through the waist beams. The struts are the supports of the beam; therefore, the south wall of the regular and irregular supporting structures can be regarded as a multisupport nonstatically indeterminate beam with one end cantilever and a multisupport nonstatically indeterminate beam, respectively. Therefore, when the lateral earth pressure acts on the diaphragm wall, the deformation modes of the south wall of the two supporting schemes are different.

Bending Moment of the Diaphragm Wall

The bending moment of the diaphragm wall is presented in Fig. 5. When the interior of the wall is pulled, the bending moment is negative. The bending moment of the irregular supporting structure is larger than that of the regular supporting structure, in particular, for the upper part of the south wall. The maximum bending moments of the diaphragm wall of the irregular and regular supporting structures are +887.3 and +830.7 kN·m, respectively (Fig. 5). There is a constraint at the top of the south wall of the irregular supporting structure, but for the regular supporting structure, no constraint exists at the top of the south wall. Thus, similar to the deflection of the wall, the bending-moment mode and amplitude of the wall of the two supporting schemes are similar except for at the upper part of the south wall. Because of the lack of constraint at the top of the south wall, the bending moment at the upper part of the south wall of the regular supporting structure is much larger than that for the irregular supporting structure (Fig. 5).

Safety Factor of the Diaphragm Wall

To evaluate the mechanical performance of the diaphragm wall, the ratio between the design limit value and the calculated working

Table 1. Geotechnical properties employed in the study

Soil layer	Unit weight (kN·m^3)	M	λ	K	μ	e_0	c' (kPa)	Φ' (°)	E (kPa)
Backfill	19.0	1.20	0.0293	0.0036	0.35	1.12	—	—	—
Silty clay	19.8	1.29	0.0312	0.0065	0.35	0.71	—	—	—
Sandy gravel	23.0	—	—	—	0.30	0.82	0	35	150×10^3
Silty clay	19.8	1.38	0.0445	0.0098	0.35	0.76	—	—	—
Argillaceous siltstone	22.8	—	—	—	0.28	0.64	200	32	500×10^3

Note: M = slope of critical state line ln q–p' space for MCC; λ and κ = compression and recompression values for MCC, respectively; μ = Poisson's ratio; e_0 = initial void ratio; c' = effective cohesion; Φ' = effective friction angle; and E = Young's modulus.

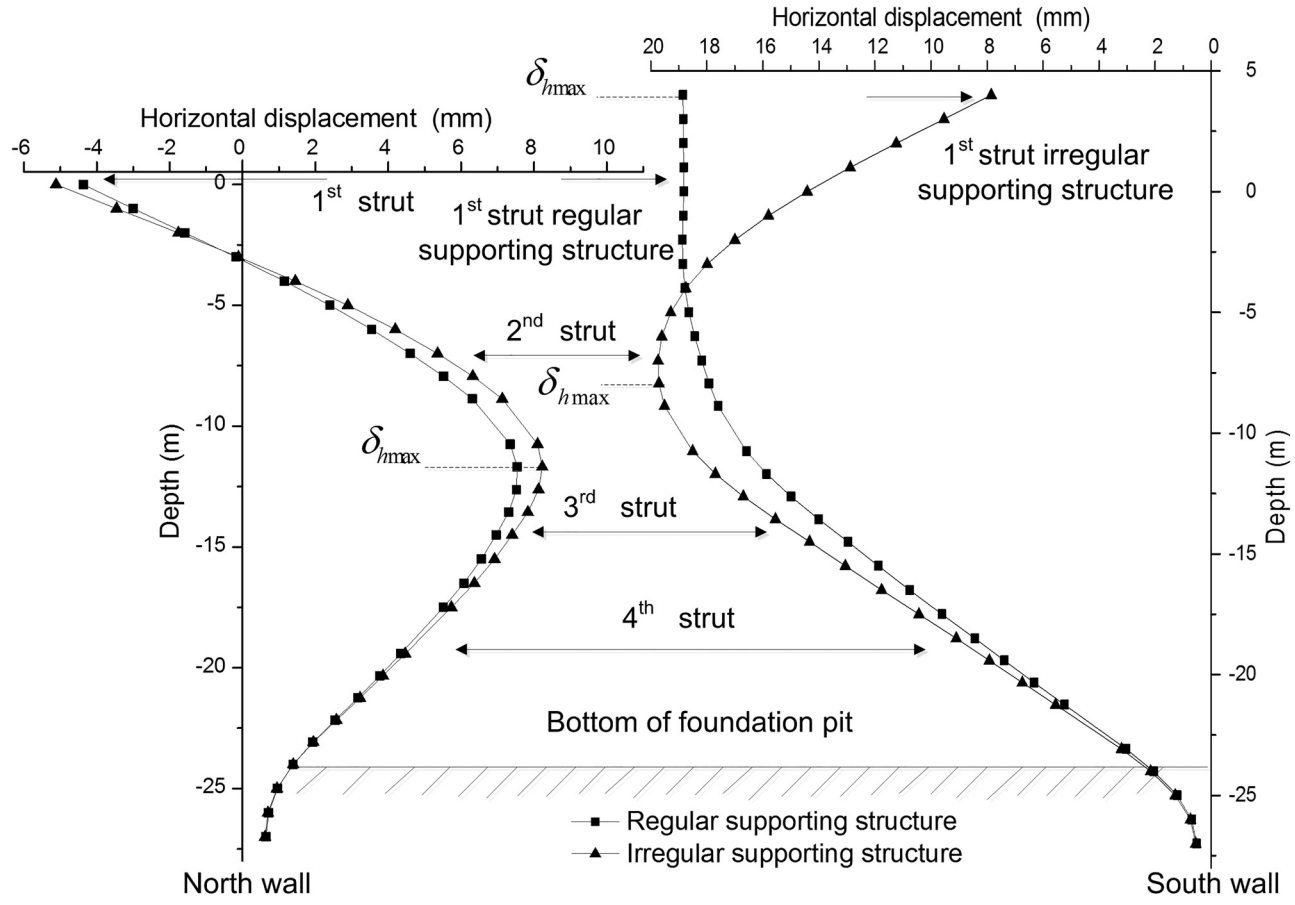

Fig. 4. Horizontal displacement curve of the diaphragm wall.

value of the diaphragm wall bending moment is defined as the safety factor. The design limit value of the diaphragm wall bending moment was calculated based on the reinforcement of the diaphragm (Shi et al. 2011; MOHURD 2015). The safety factors of the diaphragm wall for the irregular and regular supporting structures are presented in Table 2. Table 2 indicates that the safety factor of the diaphragm wall of the regular supporting structure is slightly larger than that for the irregular supporting structure except for that for the upper part of the south wall. The minimum safety factors of the diaphragm wall of the irregular and regular supporting structures are 1.1 and 1.2, respectively, and these structures are all located 11.4 m BLGS. Because of the lack of any constraint at the top of the south wall, the safety factor of the upper part of the south wall of the regular supporting structure is much larger than that for the irregular supporting structure (Table 2). The minimum safety factor of the diaphragm wall in different construction stages was calculated, and the results are presented in Table 3. The minimum safety factor of the north diaphragm wall appears at Step 6, whereas that of the south wall appears at Step 10. When a deep excavation bears different elevations at two sides, the dangerous construction stage for the high-elevation side would be at the end of the excavation, and for the low-elevation side, the dangerous construction stage may be during the excavation of a medium depth.

Performance of the Erect Column Piles

The vertical displacement at the top of the erect column piles in different excavation stages was recorded, and the results are presented in Fig. 6. When the erect column piles are uplifted, the vertical displacement of the erect column piles is positive. The elevation of the top of the erect column piles for the two supporting schemes is different (Fig. 2). Thus, the vertical displacement of the erect piles of the regular supporting structure is not affected by the excavation unloading of the topsoil with a thickness of 4 m. Therefore, the

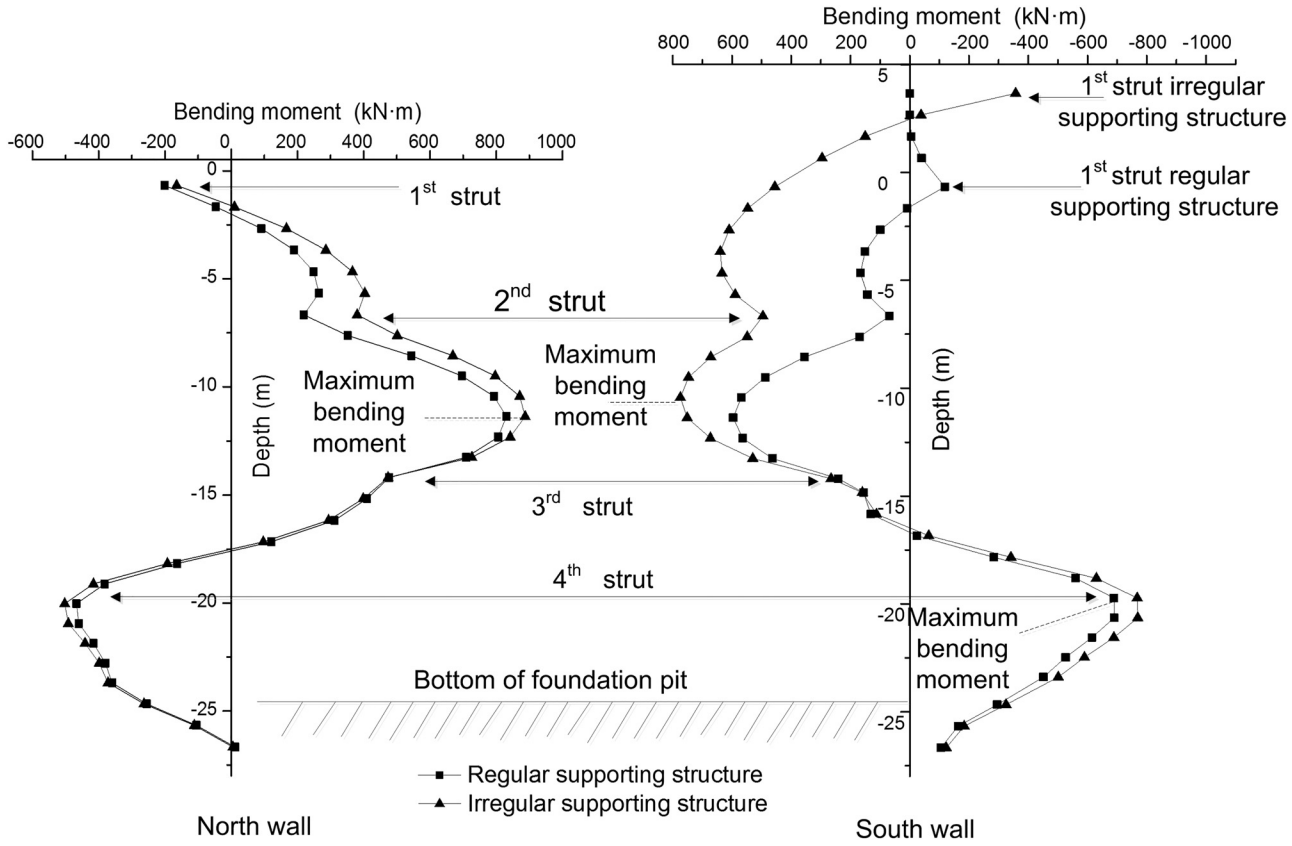

Fig. 5. Bending moment of the diaphragm wall.

Table 2. Safety factor of the diaphragm wall

	Irregular supporting structure		Regular supporting structure	
BLGS (m)	North wall	South wall	North wall	South wall
3.7	—	2.8	—	1,068.7
1.7	—	10.9	—	286.8
−0.7	5.8	2.4	6.3	31.5
−5.7	3.0	2.2	4.9	33.9
−7.6	2.4	2.8	3.6	28.6
−11.4	1.1	2.1	1.2	3.3
−13.3	1.7	5.5	1.6	7.4
−16.8	9.8	19.3	10.6	20.7
−18.8	6.9	5.8	7.2	7.3
−22.5	4.1	5.2	4.2	6.7
−24.7	4.5	13.5	5.7	15.6
−26.7	166.7	32.2	223.7	34.3

Table 3. Minimum safety factor of the diaphragm wall for different analysis steps

	Irregular supporting structure		Regular supporting structure	
Step	North wall	South wall	North wall	South wall
4	1.34	2.84	1.80	3.52
6	1.09	2.87	1.24	3.86
8	1.11	2.81	1.27	3.73
10	1.31	2.13	1.53	3.31

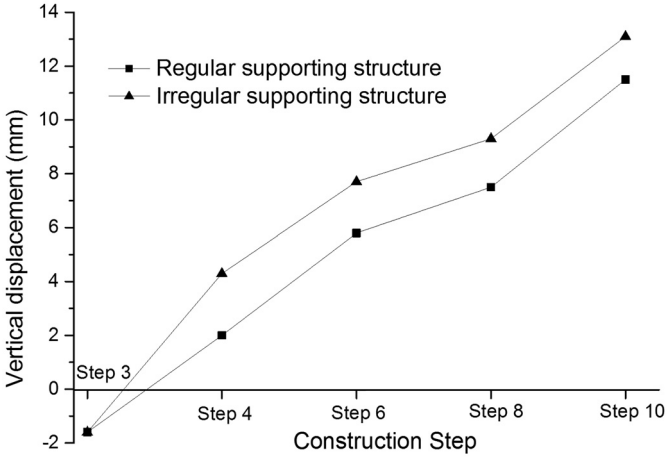

Fig. 6. Vertical displacement of the top of the erect column piles.

vertical displacement of the erect column piles of the regular supporting structure is smaller than that of the irregular supporting structure (Fig. 6).

The final horizontal displacement of the erect column piles is presented in Fig. 7. When the erect column piles deform toward the low-terrain side, the horizontal displacement is positive. The two ends of the struts are rigidly connected to the diaphragm wall through the waist beams; the neutral position of the struts is rigidly connected to the erect column piles. The horizontal displacement of the south wall at the same depth is larger than that of the north wall (Fig. 4), causing the erect column piles to deform toward the low-terrain side of the two supporting schemes (Fig. 7). Further, the

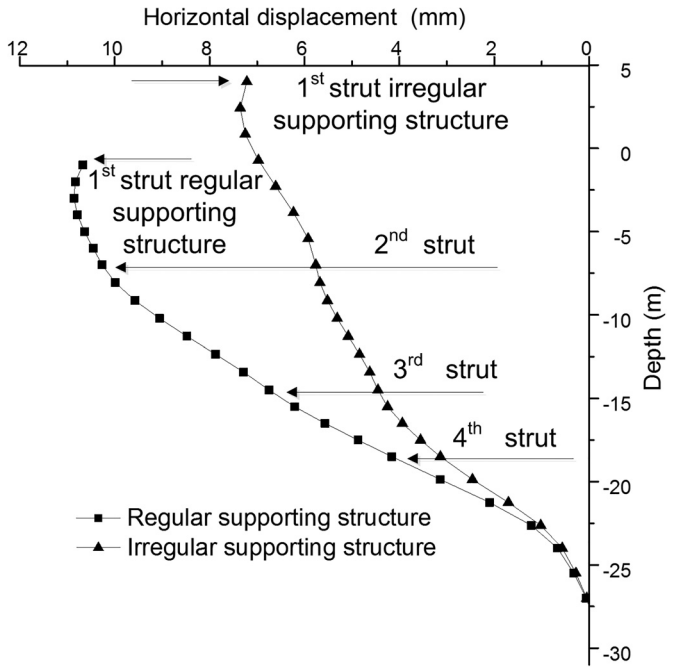

Fig. 7. Horizontal displacement of the erect column piles.

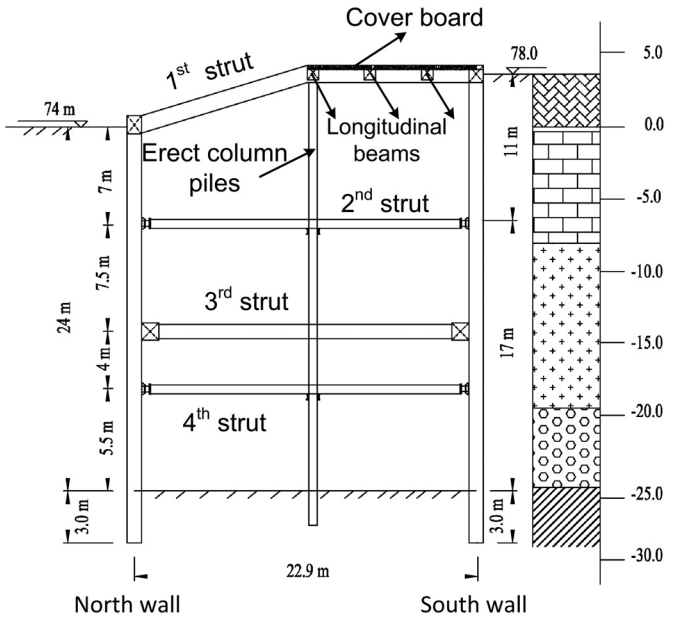

Fig. 8. Optimal supporting scheme for Shazitang metro station.

horizontal displacement of the upper part of the south wall of the regular supporting structure is much larger than that of the irregular supporting structure. Thus, the horizontal displacement of the erect column piles of the irregular supporting structure is smaller than that of the regular supporting structure (Fig. 7).

Optimal Supporting Scheme for Shazitang Deep Excavation

The deformations and safety factors of both the regular and irregular supporting structures satisfy the requirements of the code in China (MOHURD 2012). However, the deformation of the diaphragm wall of the regular supporting structure exhibits a cantilever deformation mode. When a diaphragm wall has a cantilever deformation, a triangular settlement trough on the surface (e.g., Peck 1969; Ou et al. 1993; Hsieh and Ou 1998) exerts considerable influence on the surrounding buildings. It is worth noting that the Shazitang metro station is located below Huangtuling Road (Fig. 1). To ensure the regular operation of road traffic on Huangtuling Road, the semicovered excavation is more suitable. However, the regular supporting structure is suitable for cut-and-cover construction, and it is not suitable for semicovered construction. Thus, the irregular supporting structure is the optimal supporting scheme for the Shazitang deep excavation (Fig. 8). The deep excavation in the semicovered area (Fig. 1) was performed using the following construction process (Fig. 9):

- *Step 1*: construct the south wall, uplift the piles, and erect column piles;
- *Step 2*: install the first straight bracing, longitudinal beams, and cover board;
- *Step 3*: build the north wall and the first inclined bracing;
- *Step 4*: excavate the first floor space;
- *Step 5*: install the second strut;
- *Step 6*: excavate the second floor space;
- *Step 7*: install the third strut;
- *Step 8*: excavate the third floor space;
- *Step 9*: install the forth strut;
- *Step 10*: excavate the fourth floor space; and
- *Step 11*: construct the bottom plate.

Numerical Performance of the Irregular Support Structure Subjected to Asymmetric Loading

Considering the cover board, longitudinal beams, and vehicle load (Kwon and Elnashai 2017), a new 3D FE model (Fig. 10) was established to investigate the performance of the irregular supporting structure subjected to asymmetric loading. The vehicle loads were equivalent to a uniform static distributed load of 40 kPa according to the simplification method in a Chinese code (MOT 2015).

Deflection of the Diaphragm Wall

The horizontal displacement curve of the diaphragm wall is presented in Fig. 11. To better understand the performance of the irregular supporting structure subjected to asymmetric loading, two excavation numerical models of symmetrical foundation excavations with excavation depths of 24 and 28 m were established. When the excavations faced the same elevation at two sides, the diaphragm wall exhibited a parabolic deformation mode (Fig. 11).

Generally, the unloading effect of the soil excavation leads to deformations (both horizontal and vertical) and changes in the stresses behind the wall. The earth pressure on the retaining structures gradually increases with the excavation. Fig. 11 indicates that the horizontal displacement of the diaphragm wall continuously develops with an increase in the excavation depth. The south wall of the irregular supporting structure exhibits a compound deformation mode and leans toward the interior of the excavation (Fig. 11). The δ_{hmax} of the south wall is 19.1 mm, representing 0.07% H_e (H_e is the depth of the excavation). At the north side, the lower part of the north wall leans toward the interior of the excavation; however, the upper part of the north wall moves toward the outside of the deep excavation. The δ_{hmax} of the upper part of the north wall is 8.6 mm, representing 0.036% H_e, which is located at the top of the wall. The δ_{hmax} of the lower part of the north wall is 10 mm, representing 0.04% H_e, which is located 11.7 m BLGS, at 0.49 H_e.

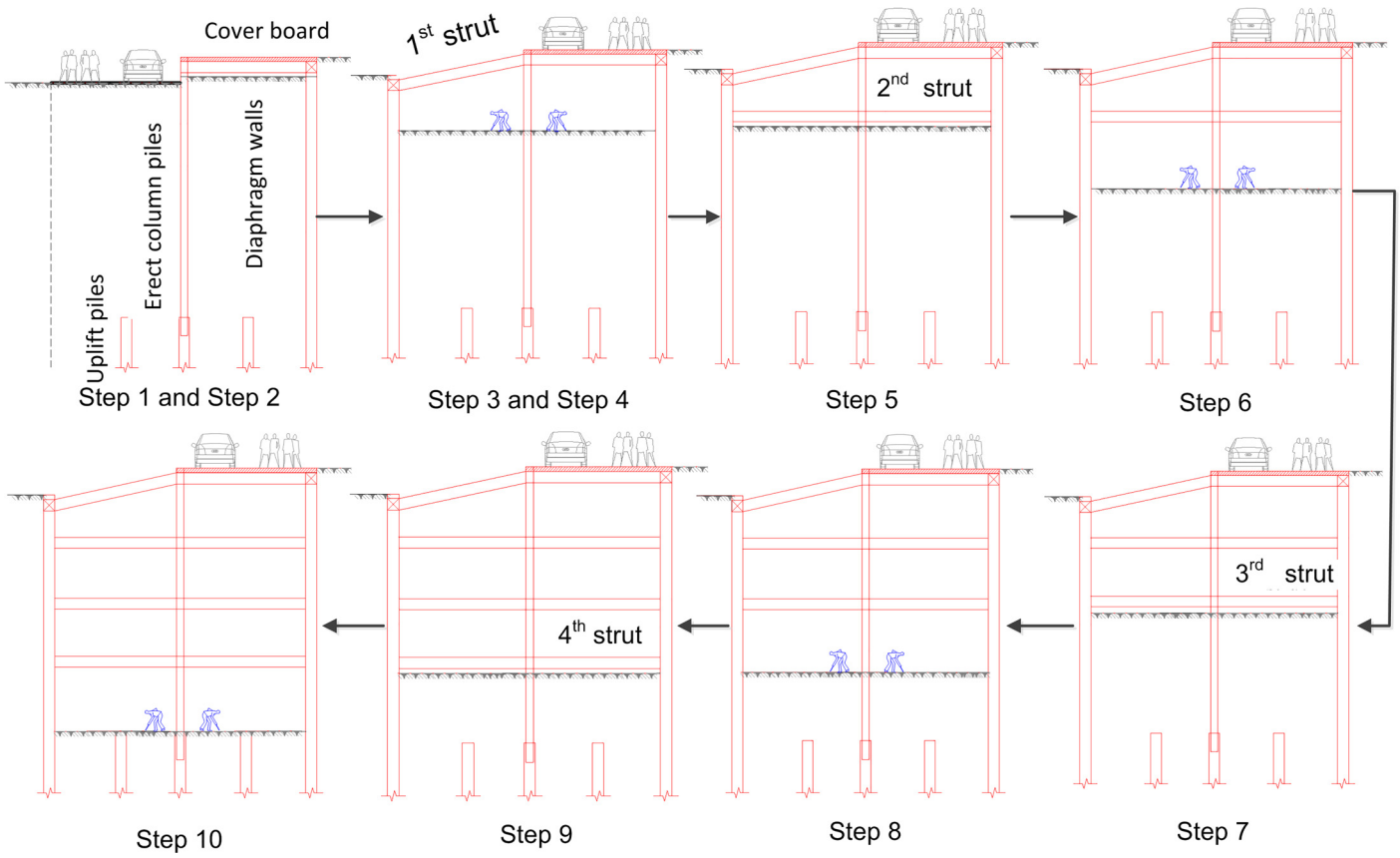

Fig. 9. Construction procedure.

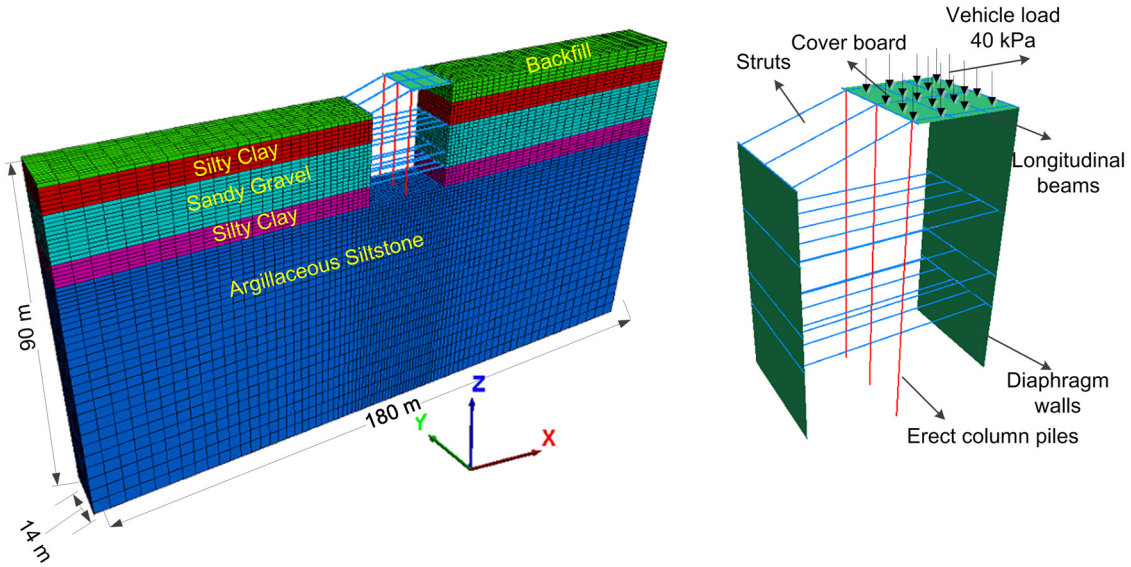

Fig. 10. 3D finite-element model.

The maximum horizontal wall displacement of the excavations in Changsha correspond to the low values with respect to the range reported by Clough and O'Rourke (1990), Leung and Ng (2007), or Moormann (2004) for similar cases of excavation (δ_{hmax} ranges from 0.15% to 0.2% H_e). This low value of the normalized maximum retaining wall deflections can be attributed to the larger stiffness of the diaphragm wall and favorable geological conditions (compared with other types of retaining walls recorded in databases). After the final excavation depth was reached, the maximum deflections of the wall occurred within a few meters above the final excavation level, potentially as a result of the geological conditions.

Compared with symmetric deep excavation, the wall deflection of asymmetric excavations is peculiar. For an asymmetric deep excavation, the diaphragm wall at the higher-terrain side

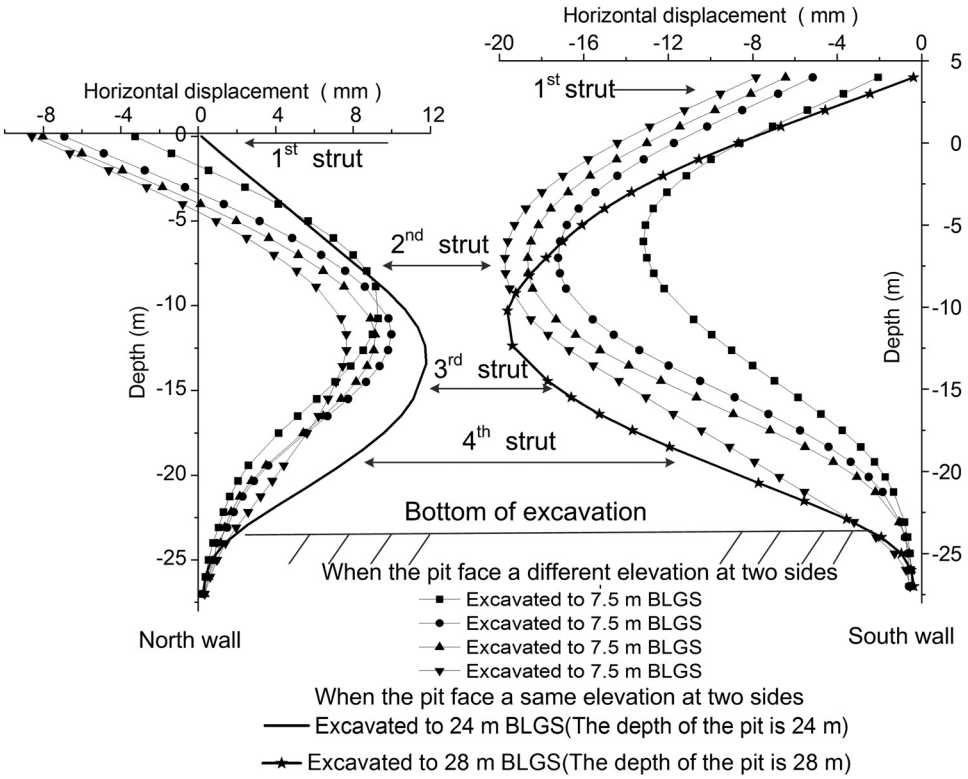

Fig. 11. Horizontal displacement of the diaphragm wall during construction.

exhibits a compound deformation mode. At the lower-terrain side, the deflection of the wall exhibits a parabolic deformation mode, which is pushed to the outside of the excavation by a certain distance. In other words, the lower part of the diaphragm wall leans toward the interior of the excavation; however, the upper part of the diaphragm wall moves toward the outside of the deep excavation. There are two main reasons for the peculiar deformation mode of the diaphragm wall. First, the lateral earth pressure is shared by the diaphragm wall and struts. Because of the terrain on the south side of the foundation excavation is higher than the north side (Figs. 1 and 8), the earth pressure on the south wall of the foundation excavation is larger than that on the north wall. The two ends of the struts are rigidly connected to the diaphragm wall through the waist beams. Thus, the lateral earth pressure on the south wall will act on the north through the struts, making the upper part of the north wall deform toward the outside of the excavation. Because of the increased lateral earth pressure on the north wall along the depth direction, the lower part of the diaphragm wall leans toward the interior of the excavation. Second, as seen from Fig. 8, the first strut of the irregular supporting structure is composed of straight bracing and inclined bracing, which leads to the stiffness of the first strut being smaller than that of the regular straight strut. Because of the low stiffness of the first support, the diaphragm at the higher-terrain side exhibits a compound deformation mode.

The numerical results show that the deformation mode of the diaphragm wall of the excavation with asymmetric loading is different from that for a symmetrical deep excavation, as presented in Fig. 12. The upper part of the north wall appears to drift toward the side with a lower elevation, and the lower part of the north wall appears to lean toward the inside of the deep excavation. At higher elevation levels (south), the diaphragm wall exhibits a compound deformation behavior (Long 2001).

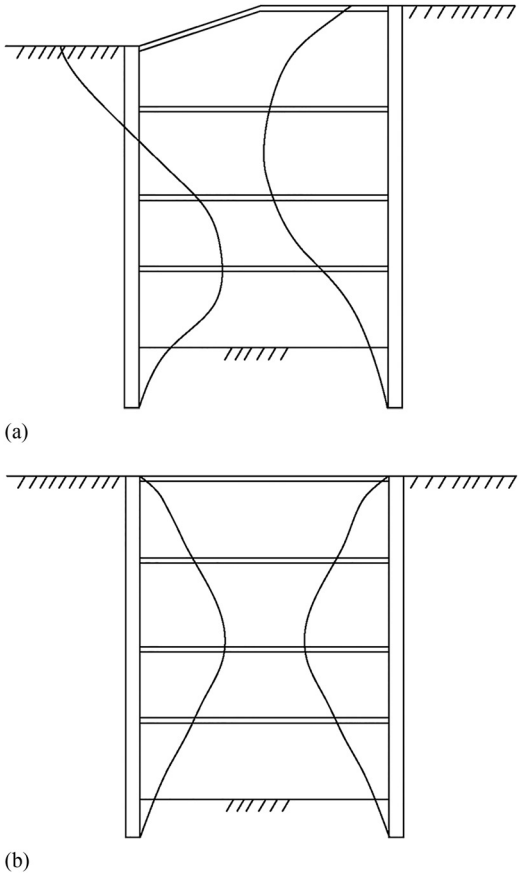

Fig. 12. Comparison of deformation modes of diaphragm wall under (a) asymmetric; and (b) symmetric loadings.

Performance of the Erect Column Piles

Fig. 13 presents the vertical displacement curve at the top of the erect column piles in different excavation stages. Because of the deadweight, vehicle loads, and excavation unloading, the erect column piles appear to change from settlement to heave (Fig. 13). As presented in Fig. 13, the erect column piles appear to be sinking before being excavated to 7 m BLGS. After that, the erect column piles appear uplifted and develop continuously with an increase in the excavation depth. The final vertical displacement is 9.3 mm, which corresponds to 0.03% H_e. Compared with the final vertical displacement of erect column piles (0.05%–0.3%) record by Tan and Wang (2013), the vertical displacement of the irregular supporting structure subjected to asymmetric loading is lesser. Because of the effect of the vehicle load and deadweight, the column presents settlement characteristics at the early excavation stage. Influenced by excavation unloading, the erect column piles present uplift characteristics at the later excavation stage.

The horizontal displacement along the depth direction of the erect column piles was recorded, and the results are presented in Fig. 14. The two ends of the struts are rigidly connected to the diaphragm wall through the waist beams; the neutral position of the struts is rigidly connected to the erect column piles. The results in Fig. 14 indicate that the horizontal displacement of the south wall at the same depth is larger than that of the north wall. Fig. 14 reveals that the erect column piles move toward the lower side. The horizontal displacement of the erect column piles develops continuously with an increase in the excavation depth. The horizontal deformation of the erect column piles appears to have a bulge shape, and the maximal displacement is 12.7 mm, located at 3 m BLGS. For the design of the erect column piles of an asymmetrical deep excavation, the transverse loading should be considered (Frank 2017).

Field Performance of the Irregular Supporting Structure

Field Monitoring

A series of systematic field tests was performed for the deep excavation to monitor the performance of the irregular supporting structure during the construction process. The monitored items included the settlement of the erect column piles and horizontal displacement of the diaphragm wall. Several monitoring instruments were installed around the excavation, including surface settlement points and inclinometers. Fig. 15 presents the original appearance of the site construction.

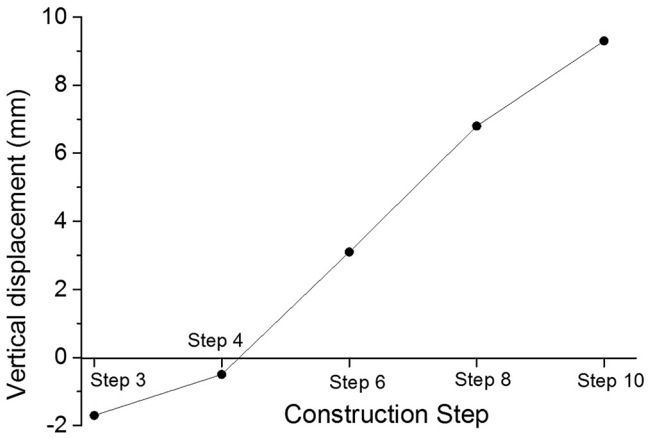

Fig. 13. Vertical displacement of erect column piles during construction.

Deflection of the Diaphragm Wall

A comparison of the results of the field measurements and numerical simulations of the horizontal displacement of the diaphragm wall is presented in Fig. 16. A reasonably good agreement can be seen between the measured and calculated horizontal displacements. The deformation mode and amplitude of the measured diaphragm wall are similar to, but not the same as, those obtained numerically. This is mainly attributable to the influence of the groundwater and uncertain construction loads not being considered in the numerical analysis.

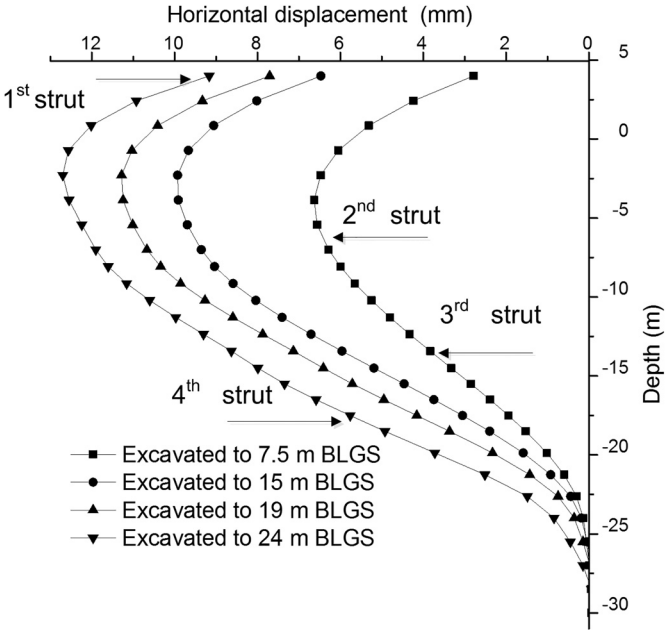

Fig. 14. Horizontal displacement of erect column piles during construction.

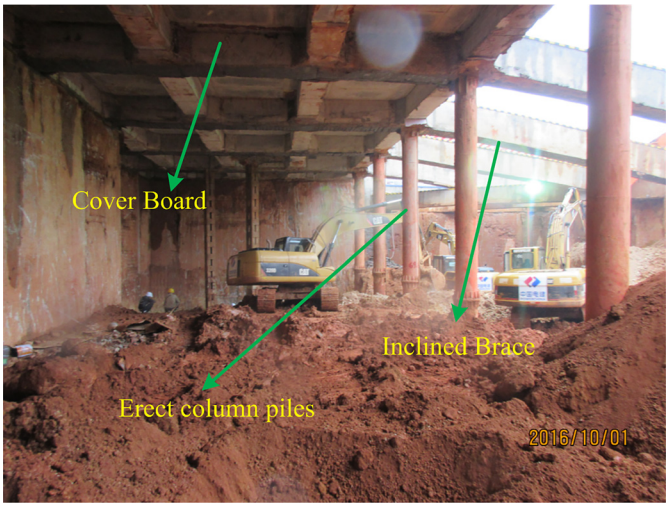

Fig. 15. First inclined struts.

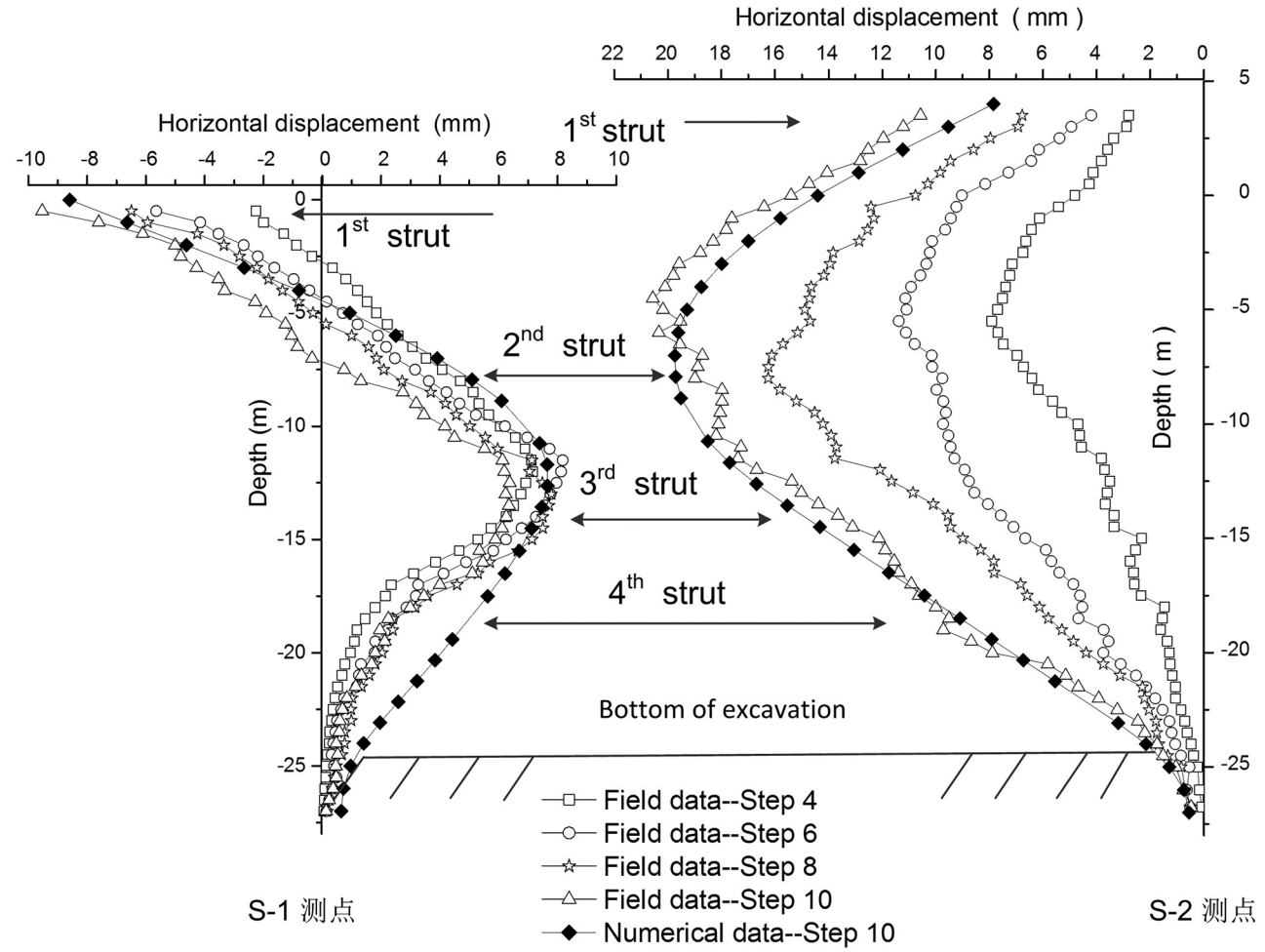

Fig. 16. Horizontal displacement of the diaphragm wall.

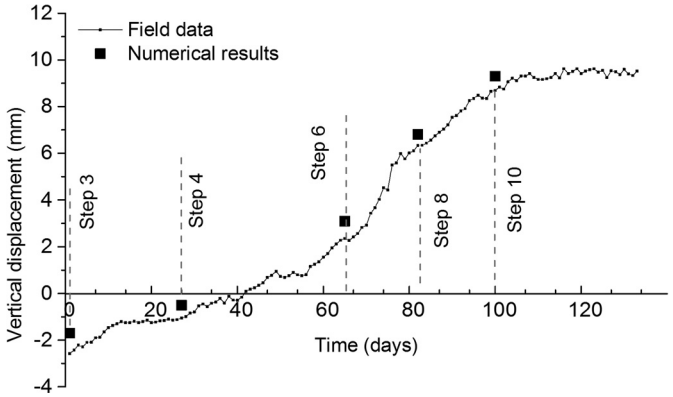

Fig. 17. Vertical displacement of erect column piles.

Vertical Displacement of the Erect Column Piles

Fig. 17 presents the vertical displacement of the erect column piles during the construction process. The data on vertical displacement in Fig. 17 reveal that the numerical results compare quite well with the field-test results. The maximum vertical displacement is 9.6 mm, pertaining to 0.03% H_e. In the precipitation stage, the relative motion between the piles and soil caused by the osmotic consolidation subjects the erect column piles to negative friction (Kavitha et al. 2016). Therefore, precipitation will increase the settlement value of the erect column pile. During construction, uncertain construction loads act on the erect column piles, resulting in suppression of the upliftment of the erect column piles. Because the numerical simulation does not take into account the effects of precipitation and uncertain construction loads, the settlement values of the measured erect column piles are larger than those obtained numerically, whereas the uplift values are less than those obtained numerically.

Conclusions

This study, using numerical analyses and field measurements, investigated the performance of a deep excavation with an irregular supporting system subjected to asymmetric loading. The following major findings and conclusions can be obtained:

1. The numerical results illustrate that the deformation and the safety factor of both the regular and irregular supporting schemes satisfy the requirements of the design code. However, the deformation of the diaphragm wall of the regular supporting structure presents a cantilever deformation mode, whereas the irregular supporting structure can be built with a cover board on the straight bracing as a temporary pavement to reduce the impact of the construction on traffic. The irregular supporting structure proves to be a suitable option for deep excavation when subjected to asymmetric loading in congested city areas.

2. The wall deflection of the asymmetric deep excavation support system is peculiar compared with that of a symmetric deep excavation. Because of the low stiffness of the first strut, the diaphragm wall at the higher-terrain side exhibits a compound deformation mode, whereas the deflection of the wall at the lower-terrain side exhibits a parabolic deformation mode and is pushed to the outside of the excavation by a certain distance. At the lower-terrain side, the lower part of the diaphragm wall leans toward the interior of the excavation, whereas the upper part of the diaphragm wall moves toward the outside of the deep excavation. The maximum horizontal wall displacement of the supporting structure is generally lower than the ranges reported in the case history; this result can be attributed to the larger stiffness of the diaphragm wall and favorable geological conditions in this case.
3. Influenced by vehicle loads, deadweight, and excavation unloading, the erect column piles appear to change from settlement to heave, and the final vertical displacement of the erect column piles is less than that reported in existing literature. The interaction between the erect column piles and struts and the asymmetric loading cause the erect column piles to deform toward the side with the lower terrain.
4. Reasonably good agreement was found between the measured and calculated results, proving that the optimal procedure of the supporting scheme is feasible. The case study shows that the irregular supporting structure can work effectively when subjected to asymmetric loading and can also help realize a semicovered excavation in limited and congested downtown areas to effectively properly solve the problem of traffic arrangements, which is extremely advantageous.

Acknowledgments

This work was supported by the National Key Research and Development Program of China (2016YFC0802500) and the National Natural Science Foundation of China (51608539).

References

Arai, Y., O. Kusakabe, O. Murata, and S. Konishi. 2008. "A numerical study on ground displacement and stress during and after the installation of deep circular diaphragm walls and soil excavation." *Comput. Geotech.* 35 (5): 791–807. https://doi.org/10.1016/j.compgeo.2007.11.001.

Chowdhury, S. S., K. Deb, and A. Sengupta. 2013. "Estimation of design parameters for braced excavation: Numerical study." *Int. J. Geomech.* 13 (3): 234–247. https://doi.org/10.1061/(ASCE)GM.1943-5622.0000207.

Clough, G. W., and T. D. O'Rourke. 1990. "Construction induced movements of in situ walls." *In Design and Performance of Earth Retaining Structures*, Geotechnical Special Publication 25, 439–470. Reston, VA: ASCE.

Desai, C. S. 2015a. "Constitutive modeling of materials and contacts using the disturbed state concept: Part 1—Background and analysis." *Comput. Struct.* 146: 214–233. https://doi.org/10.1016/j.compstruc.2014.07.018.

Desai, C. S. 2015b. "Constitutive modeling of materials and contacts using the disturbed state concept: Part 2—Validations at specimen and boundary value problem levels." *Comput. Struct.* 146: 234–251. https://doi.org/10.1016/j.compstruc.2014.07.026.

Frank, R. 2017. "Some aspects of research and practice for pile design in France." *Innovative Infrastruct. Solutions* 2 (1): 32. https://doi.org/10.1007/s41062-017-0085-4.

Hashash, Y. M. A., C. Marulanda, J. Ghaboussi, and S. Jung. 2006. "Novel approach to integration of numerical modeling and field observations for deep excavations." *J. Geotech. Geoenviron. Eng.* 132 (8): 1019–1031. https://doi.org/10.1061/(ASCE)1090-0241(2006)132:8(1019).

Hou, Y. M., J. H. Wang, and L. L. Zhang. 2009. "Finite-element modeling of a complex deep excavation in Shanghai." *Acta Geotech.* 4 (1): 7–16. https://doi.org/10.1007/s11440-008-0062-3.

Hsieh, P. G., and C. Y. Ou. 1998. "Shape of ground surface settlement profiles caused by excavation." *Can. Geotech. J.* 35 (6): 1004–1017. https://doi.org/10.1139/t98-056.

Hsieh, P. G., C. Y. Ou, and Y. L. Lin. 2013. "Three-dimensional numerical analysis of deep excavations with cross walls." *Acta Geotech.* 8 (1): 33–48. https://doi.org/10.1007/s11440-012-0181-8.

Huang, M., Y. Liu, and D. Sheng. 2011. "Simulation of yielding and stress-stain behavior of Shanghai soft clay." *Comput. Geotech.* 38 (3): 341–353. https://doi.org/10.1016/j.compgeo.2010.12.005.

Kavitha, P. E., K. S. Beena, and K. P. Narayanan. 2016. "A review on soil-structure interaction analysis of laterally loaded piles." *Innovative Infrastruct. Solutions* 1 (1): 14. https://doi.org/10.1007/s41062-016-0015-x.

Kim, D. S., and B. C. Lee. 2005. "Instrumentation and numerical analysis of cylindrical diaphragm wall movement during deep excavation at coastal area." *Mar. Georesour. Geotech.* 23 (1–2): 117–136. https://doi.org/10.1080/10641190590953728.

Kwon, O. S., and A. S. Elnashai. 2017. "Distributed analysis of interacting soil and structural systems under dynamic loading." *Innovative Infrastruct. Solutions* 2 (1): 30. https://doi.org/10.1007/s41062-017-0076-5.

Leung, E. H. Y., and C. W. W. Ng. 2007. "Wall and ground movements associated with deep excavations supported by cast in situ wall in mixed ground conditions." *J. Geotech. Geoenviron. Eng.* 133 (2): 129–143. https://doi.org/10.1061/(ASCE)1090-0241(2007)133:2(129).

Liu, G. B., C. W. W. Ng, and Z. W. Wang. 2005. "Observed performance of a deep multistrutted excavation in Shanghai soft clays." *J. Geotech. Geoenviron. Eng.* 131 (8): 1004–1013. https://doi.org/10.1061/(ASCE)1090-0241(2005)131:8(1004).

Long, M. 2001. "Database for retaining wall and ground movements due to deep excavations." *J. Geotech. Geoenviron. Eng.* 127 (3): 203–224. https://doi.org/10.1061/(ASCE)1090-0241(2001)127:3(203).

MOHURD (Ministry of Housing and Urban-Rural Development of the People's Republic of China). 2012. *Technical specification for retaining and protection of building foundation excavations.* [In Chinese.] Beijing: China Architecture & Building.

MOHURD (Ministry of Housing and Urban-Rural Development of the People's Republic of China). 2015. *Code for design of concrete structures.* [In Chinese.] Beijing: China Architecture & Building.

Moormann, C. 2004. "Analysis of wall and ground movements due to deep excavations in soft soil based on a new worldwide database." *Soils Found.* 44 (1): 87–98. https://doi.org/10.3208/sandf.44.87.

MOT (Ministry of Transport of the People's Republic of China). 2015. *Technical standard of highway engineering.* [In Chinese.] Beijing: China Architecture & Building.

Nogueira, C. D. L., F. R. D. Azevedo, and J. G. Zornberg. 2011. "Validation of coupled simulation of excavations in saturated clay: Camboinhas case history." *Int. J. Geomech.* 11 (3): 202–210. https://doi.org/10.1061/(ASCE)GM.1943-5622.0000077.

Ou, C. Y., P. G. Hsieh, and D. C. Chiou. 1993. "Characteristics of ground surface settlement during excavation." *Can. Geotech. J.* 30 (5): 758–767. https://doi.org/10.1139/t93-068.

Ou, C. Y., J. T. Liao, and H. D. Lin. 1998. "Performance of diaphragm wall constructed using top-down method." *J. Geotech. Geoenviron. Eng.* 124 (9): 798–808. https://doi.org/10.1061/(ASCE)1090-0241(1998)124:9(798).

Ou, C. Y., F. C. Teng, and I. W. Wang. 2008. "Analysis and design of partial ground improvement in deep excavation." *Comput. Geotech.* 35 (4): 576–584. https://doi.org/10.1016/j.compgeo.2007.09.005.

Peck, R. B. 1969. "Deep excavation and tunneling in soft ground. State-of-the-art report." In *Proc., 7th Int. Conf. of Soil Mechanics and Foundation Engineering*, 225–281. London: International Society of Soil Mechanics and Geotechnical Engineering.

Schwamb, T., and K. Soga. 2015. "Numerical modelling of a deep circular excavation at Abbey Mills in London." *Géotechnique* 65 (7): 604–619. https://doi.org/10.1680/geot.14.P.251.

Shao, Y., and E. J. Macari. 2008. "Information feedback analysis in deep excavations." *Int. J. Geomech.* 8 (1): 91–103. https://doi.org/10.1061/(ASCE)1532-3641(2008)8:1(91).

Shi, Y. F., J. S. Yang, W. Bai, and X. M. Zhang. 2011. "Analysis of field testing for deformation and internal force of unsymmetrical loaded foundation pit's enclosure structure close to railway." [In Chinese.] *Chin. J. Rock Mech. Eng.* 30 (4): 826–833.

Tan, Y., and M. Li. 2011. "Measured performance of a 26 m deep top-down excavation in downtown Shanghai." *Can. Geotech. J.* 48 (5): 704–719. https://doi.org/10.1139/t10-100.

Tan, Y., and D. Wang. 2013. "Characteristics of a large-scale deep foundation pit excavated by the central-island technique in Shanghai soft clay. II: Top-down construction of the peripheral rectangular pit." *J. Geotech. Geoenviron. Eng.* 139 (11): 1894–1910. https://doi.org/10.1061/(ASCE)GT.1943-5606.0000929.

Xiao, Y., H. Liu, Y. Chen, and J. Jiang. 2014. "Bounding surface model for rockfill materials dependent on density and pressure under triaxial stress conditions." *J. Eng. Mech.* 140 (4): 04014002. https://doi.org/10.1061/(ASCE)EM.1943-7889.0000702.

Yang, X., and G. Liu. 2017. "Performance of a large-scale metro interchange station excavation in Shanghai soft clay." *J. Geotech. Geoenviron. Eng.* 143 (6): 05017003. https://doi.org/10.1061/(ASCE)GT.1943-5606.0001681.

Yao, Y. P., Z. Gao, J. Zhao, and Z. Wan. 2012. "Modified UH model: Constitutive modeling of overconsolidated clays based on a parabolic Hvorslev envelope." *J. Geotech. Geoenviron. Eng.* 138 (7): 860–868. https://doi.org/10.1061/(ASCE)GT.1943-5606.0000649.

Yao, Y. P., W. Hou, and A. N. Zhou. 2008. "Constitutive model for overconsolidated clays." *Sci. China Ser. E: Technol. Sci.* 51 (2): 179–191. https://doi.org/10.1007/s11431-008-0011-2.

Yao, Y. P., W. Hou, and A. N. Zhou. 2009. "UH model: Three-dimensional unified hardening model for overconsolidated clays." *Géotechnique* 59 (5): 451–469. https://doi.org/10.1680/geot.2007.00029.

Yoo, C., and D. Lee. 2008. "Deep excavation-induced ground surface movement characteristics—A numerical investigation." *Comput. Geotech.* 35 (2): 231–252. https://doi.org/10.1016/j.compgeo.2007.05.002.

Zeng, C. F., X. L. Xue, and G. Zheng. 2017. "Effect of soil permeability on wall deflection during pre-excavation dewatering in soft ground." [In Chinese.] *Rock Soil Mech.* 38 (10): 3039–3047. https://doi.org/10.16285/j.rsm.2017.10.033.

Zhang, X., J. Yang, Y. Zhang, and Y. Gao. 2018. "Cause investigation of damages in existing building adjacent to foundation pit in construction." *Eng. Fail. Anal.* 83: 117–124. https://doi.org/10.1016/j.engfailanal.2017.09.016.

Zhao, Y., C. Liu, Y. Zhang, J. Yang, and T. Feng. 2019a. "Damaging behavior investigation of an operational tunnel structure induced by cavities around surrounding rocks." *Eng. Fail. Anal.* 99: 203–209. https://doi.org/10.1016/j.engfailanal.2019.02.023.

Zhao, Y., Y. Shi, and J. Yang. 2019b. "Study of the influence of train vibration loading on adjacent damaged tunnel." *Shock Vibr.* 2019: 1–8. https://doi.org/10.1155/2019/3417598.